Scientific Data

https://doi.org/10.1038/s41597-026-07597-2

Article in Press

High-resolution spatial transcriptomics of adult and pediatric human liver with Visium HD

Received: 18 December 2025

Accepted: 2 June 2026

Cite this article as: Hasan, F., Edgar, R.D., Atif, J. *et al.* High-resolution spatial transcriptomics of adult and pediatric human liver with Visium HD. *Sci Data* (2026). https://doi.org/10.1038/s41597-026-07597-2

Faizan Hasan, Rachel D. Edgar, Jawairia Atif, Diana Nakib, Cornelia Thoeni, Amanda Ricciuto, Blayne A. Sayed, Ian McGilvray, Gary D. Bader & Sonya A. MacParland

High-resolution spatial transcriptomics of adult and pediatric human liver with Visium HD

Faizan Hasan[1-4]*, Rachel D. Edgar[1,4]*^, Jawairia Atif[1,5], Diana Nakib[1,5], Cornelia Thoeni[6,7], Amanda Ricciuto[8], Blayne A. Sayed[1], Ian McGilvray[1], Gary D. Bader[3,4,9-12], and Sonya A. MacParland[1,5,13]^

(1) Ajmera Transplant Centre, Toronto General Research Institute, University Health Network, Toronto, Ontario, Canada
(2) Department of Medical Biophysics, University of Toronto, Toronto, Ontario, Canada
(3) Department of Molecular Genetics, University of Toronto, Toronto, Ontario, Canada
(4) Donnelly Centre, University of Toronto, Toronto, Ontario, Canada
(5) Department of Immunology, University of Toronto, Toronto, Ontario, Canada
(6) Department of Pathology and Lab Medicine, Nova Scotia Health Authority, Halifax, Nova Scotia, Canada
(7) Dalhousie University, Faculty of Medicine, Halifax, Nova Scotia, Canada
(8) Division of Gastroenterology, Hepatology & Nutrition, Hospital for Sick Children, University of Toronto, Toronto, Ontario, Canada
(9) Princess Margaret Cancer Centre, University Health Network, Toronto, Ontario, Canada
(10) Department of Computer Science, University of Toronto, Toronto, Ontario, Canada
(11) Lunenfeld-Tanenbaum Research Institute, Sinai Health System, Toronto, Ontario, Canada
(12) CIFAR Multiscale Human Program, CIFAR, Toronto, Ontario, Canada
(13) Department of Laboratory Medicine and Pathobiology, University of Toronto, Toronto, Ontario, Canada

**These authors contributed equally*
^corresponding

Address for Correspondence

r.edgar@utoronto.ca (R.D. Edgar)

s.macparland@utoronto.ca (S.A. MacParland)

Abstract

The liver is composed of diverse cell populations that coordinate essential metabolic and immune functions. Single-cell transcriptomics has advanced characterization of liver cellular composition, but dissociation of tissue to single-cells can introduce biases through the enrichment or depletion of cell types. Spatial transcriptomics is a complementary approach to avoid inherent bias for cell populations and to add important spatial context. The Visium HD spatial transcriptomics technology from 10X Genomics enables high-resolution spatial mapping of gene expression in tissue samples with a bin width of 2µm enabling quantification of transcripts at a sub-cellular resolution. We applied Visium HD to three healthy human liver donor samples, from two adult and one pediatric donor. We identified cell types by clustering 8µm bins and integration with single-cell reference maps. Differential expression analyses identified spatially distinct gene expression resulting in development of a high-resolution map of the liver. This resource provides cell-level and spatially-resolved insights into the cellular and anatomical heterogeneity of the liver to serve as a resource for researchers to identify disease-specific spatial signatures and novel therapeutic targets.

Background and Summary

The liver plays a critical role in metabolism and immune function. These crucial roles are diminished in chronic liver diseases, leading to over two million deaths annually worldwide due to liver failure[1]. Single-cell transcriptomics has provided insights into the cellular composition of livers in health and disease, but is biased due to cell type-specific enrichment or depletion during the single-cell dissociation process. Previous work has highlighted difficulties in capturing specific populations such as cholangiocytes and hepatocytes[2]. In the cells captured, the process of dissociation has been shown to impact gene transcription[3].

Spatial transcriptomics is a promising approach that does not have inherent bias for cell populations, and adds important spatial context. Spatial transcriptomics has been shown to capture important patterns of zonation in the human liver[4], a dynamic feature important for understanding basic liver functions and alterations in liver disease processes. Until recently, spatial transcriptomic technologies have been low-resolution (Visium, 55µm) potentially mixing signals from multiple cells and multiple cell types. The latest spatial transcriptomic technology from 10X Genomics, Visium HD, enables high-resolution (2µm) spatial mapping of gene expression in tissue samples, offering a sophisticated platform for exploring the cellular composition of the liver.

Here we assayed samples from three neurologically deceased donor livers, with no evidence of histopathological liver disease. This data is at higher resolution than previous whole-transcriptome spatial datasets of healthy human liver[5]. The increased resolution, achieved using the probe-based Visium HD platform rather than whole-transcriptome capture, enables the identification of rare and transcriptionally distinct cell populations within the liver zonation structure. While we do see variation in data quality across the three samples, we provide these data as a resource for better understanding of the cellular and spatial liver heterogeneity.

Methods

Figure 1A provides an overview of the liver spatial transcriptomics data generation which involves the collection of human liver tissue, preparing tissue sections, and Visium HD sample processing.

Table 1. Spatial transcriptomic sample information

Sample	Age	Sex	Tissue	Storage	Reads	Sequencing saturation	Spacer Ranger version	Associated data previously published
C107	51	M	Caudate	Stored for 1 year at 4°C	929,681,741	58.9%	3.0.0	None
C95	47	F	Caudate	Stored 2 years; 1 year room temperature 1 year 4°C	333,465,658	81.0%	3.0.0	Xenium spatial[6]

C113	15-19	M	Right lobe	Stored for 2 years at 4°C	225,446,253	93.1%	3.0.1	Dissociated single-cell[6]

Human Liver Sample Collection

Healthy human liver tissue from the caudate or right liver lobe was obtained from neurologically deceased donor livers (**Table 1**). Donated livers had no evidence of histopathological liver disease supported by the hematoxylin and eosin (H&E) staining of the samples[7]. However, liver tissue from neurologically deceased donors may exhibit transcriptional changes related to hemodynamic instability, inflammatory activation, or damage from ischemia events[8]. These factors represent a potential limitation when interpreting transcriptional patterns in otherwise healthy liver tissue.

Fresh human liver samples were collected at the Hospital for Sick Children and Toronto General Hospital transplant centres. Liver tissue was prepared for Visium HD spatial transcriptomics by first processing into formalin-fixed, paraffin-embedded (FFPE) blocks which were then sectioned into 5µm thick slices and mounted onto 6.5mm by 6.5mm Visium HD slides (Visium HD v1 - FFPE; probe set v2.0) following the Visium HD Gene Expression User Guide.

Samples were sequenced on an Illumina NovaSeq X system. The Visium HD spatial transcriptomic data were sequenced to the depths between 300 - 950 million reads (**Table 1**). As sample C107 was initially only sequenced to a saturation of 34.4% the library was sequenced again for a final saturation of 58.9%. Reads were mapped to the human transcriptome (GRCh38-2020-A) and expression was quantified using Space Ranger software (**Table 1**). One sample (C113) was part of a tissue microarray (TMA) with three diseased liver samples included in the Visium HD capture area. Those diseased samples are not included in the sequencing data presented here, but are present in image files to enable future re-processing of the samples if needed.

Ethics Statement

Healthy adult samples were collected with institutional ethics approval from the University Health Network (REB# 14-7425-AE) and the healthy pediatric sample through the Hospital for Sick Children (REB# 1000064039). This research was conducted in accordance with the Declarations of Helsinki and Istanbul, with written informed consent obtained from participants or, for pediatric or deceased donors, from their legal guardians or representatives. Participants or their guardians/representatives consented to the collection, generation, and sharing of genomic data for research purposes. Consent procedures addressed potential privacy risks associated with genomic data sharing. The approved ethics protocols allowed for dissemination of de-identified data under an open license.

Annotation of Cell Type in 8µm Bins

Of the three samples processed, C107 had markedly higher quality, with twice as many genes and transcripts captured per bin (**Fig. 1b-d**). With only a few samples, it is uncertain why there was such variability in quality, but some sample storage information is available in **Table 1**.

To annotate bins with a cell type, an existing liver single-cell RNA-seq reference was mapped onto the spatial data (**Fig. 2a**). The published human liver single-cell reference used included 89,637 cells, with 27 annotated cell types[4]. The Robust Cell Type Decomposition (RCTD)[9] software was used to estimate cell type mixtures in spatial spots. To limit technical artefacts, low-quality bins with fewer than 100 UMIs were labelled as such in the bin annotation and filtered out from subsequent analysis (this removed 13% of all bins for C107 which were mainly around the edges and in the lumen **Fig. 1di**) before cell type annotation of bins (**Fig. 2b**). Spot class labels were assigned to bins using RCTD. The RCTD spot class "*singlet*" refers to bins predicted to contain only one cell type, whereas "*doublet-certain*" and "*doublet-uncertain*" refer to bins predicted to contain two cell types. Out of the high-quality bins, 67% were assigned an RCTD spot class and a cell type annotation (**Fig. 2bc and Fig. 3a-d**). As noted, samples C95 and C113 were of lower quality than C107, with only 47.2% and 8.9% of their 8 µm bins, respectively, passing the RCTD quality threshold of a minimum of 100 UMIs. Despite this reduced coverage, the proportions of cell types in the high-quality bins were significantly correlated between C107 and the other two samples, suggesting biological signals are still present in these samples (**Fig. 3e**). For the 33% of bins not well mapped to a cell type in the single-cell reference (i.e. RCTD "*rejects*"), these bins were clustered spatially using BANKSY[10] spatially aware clustering followed by manual annotation of distinct cell types using known cell type markers and spatial context (**Fig. 3 and 4**). Most RCTD "*rejects*" (63%) could be annotated as hepatocytes, using the BANKSY clusters and known markers. Although correlated biological signals were observed across samples, detailed downstream analyses were focused on sample C107 due to its substantially higher data quality.

Liver tissue has defined spatial structure[11] with hepatocytes arranged along a portal-to-central axis that generates metabolic and transcriptional gradients, a phenomenon known as liver zonation. We constructed a liver zonation axis in this data by dividing all bins into nine zonation layers, using a previously described method[12]. In brief, hepatocyte zonation scores were calculated using established marker genes[12] and the *AddModuleScore* function from Seurat[13–15]. Bins were stratified into nine layers based on these scores. Based on these zonation scores individual bins were split into nine zonation layers. This zonation annotation was then smoothed by reassigning the zonation layer for a bin to the median zonation layer of its neighboring bins, as previously described[12]. Layer 1 corresponds to the most pericentral regions (near the central vein), layer 8 to the most periportal regions (near the portal triad), and layer 9 to regions more dense in fibroblasts and mainly but not exclusively periportal. For hepatocytes, the zonation layer was appended to the cell type name in the final annotation. Zonation of all genes across these layers was measured as differential expression between layers using the *FindAllMarkers* function from Seurat[13–15] (with the default parameters except setting *logfc.threshold* = 0 and *min.pct*=0). Zonated genes were identified using a Wilcoxon rank-sum test, with significance defined as a Bonferroni-adjusted p-value < 0.005 and an absolute log2 fold change > 1.

Pairing Visium HD transcriptional information and H&E images enabled the examination of structural features in the human liver. Lumen regions were identified in the H&E image based on colour intensity. The space in the image not covered by tissue (around the tissue section or in lumens) was identified by clustering the pixels of the H&E image by colour (k-means; k=5). The lightest coloured cluster captured this empty space. Then the empty space pixels were grouped spatially by distance from each other, using the graph_from_adjacency_matrix function in

igraph[14] Connected groups of empty space pixels were then identified within this graph using the *components* function, implementing a connected components algorithm, with default parameters. This identified 110 lumen regions within the tissue. Lumen regions were classified by size to distinguish small sections of sinusoid (<150 pixels), small lumen (<600 pixels), and large lumen (>600 pixels). This translated to a mean diameter of 46µm for small lumen and 129µm for large. These lumen identified from the H&E image were overlaid with the 8µm bin coordinates to assign bins to lumen. Proximity to lumen regions was defined as: within 16µm ("adjacent") and 80µm ("proximal"). Cell composition was then compared between regions adjacent or proximal to either small or large lumen (**Fig. 5a-d**). Fibroblast and hepatic stellate cell abundance significantly varied by proximity to the lumen (adjacent vs. proximal; two-way ANOVA, $p<0.05$), but was not significantly dependent on lumen size (large vs. small).

Cell annotation was performed at the 8µm bin resolution across the entire sample (**Fig. 1b-c**), which may limit the resolution of small cell types, as reflected by the number of 8 µm bins annotated as doublets (**Fig. 2b)**. To capture smaller cell types, at one representative central vein region, RCTD was run on 2µm bins with a cut off for low UMI of 20 (**Fig. 6a**). At this central vein, cells lining the vein were annotated by RCTD as endothelial cells and these cells were visually distinct in the H&E images (**Fig. 6bc**). At this same central vein region, no 8µm bins at the lining of the veins were annotated as endothelial cells (**Fig. 6de**). The ability to annotate the expected endothelial cells lining this vein demonstrates the utility of the 2µm bin resolution to identify smaller cells that may be missed at 8µm.

As bile ducts are made up of adjacent cholangiocytes, we identified bile ducts by grouping neighboring bins annotated as intrahepatic cholangiocytes (**Fig. 7ab**). A cell–cell adjacency matrix, based on Euclidean distances between cholangiocytes, was converted into an undirected graph using the *graph_from_adjacency_matrix* function in igraph[16]. As before, connected groups of cholangiocytes using the *components* function with default parameters. Of the 368 connected components of cholangiocytes, those containing more than 20 bins were classified as large bile ducts, those with 2–20 bins as small bile ducts, and groups with fewer than 2 bins were excluded as potential technical artifacts. This translated to a mean diameter of 26µm for small ducts and 82µm for large (**Fig. 7C**).

Validation of Gene Expression Measurements by Immunohistochemistry

Immunohistochemical images were obtained from the Human Protein Atlas (https://www.proteinatlas.org) and the annotation of central and portal veins were confirmed by a liver pathologist (CT). The representative immunohistochemistry (IHC) stain shown is for: HAL - antibody HPA038547 patient id 2429; CYP1A2 - antibody CAB016531 patient id 3378.

Data Record

Data are available[17] NCBI Gene Expression Omnibus (GEO) under accession number GSE311383. The associated H&E images and annotation of the 8 µm bins[7] are available at: https://doi.org/10.5281/zenodo.19609466

Technical Validation

To technically validate the data, we assessed its ability to capture a strong expected biological signal. In liver spatial transcriptomics, one of the strongest expected signals is hepatocyte zonation. We therefore wanted to validate the ability of the Visium HD to capture hepatocyte zonation. capture this pattern. Differential expression analysis of Visium HD bins revealed clear periportal and pericentral markers (**Fig. 8a**). Fold-change values were calculated by comparing all 8 µm bins assigned to a given zonation region against all other bins (**Fig. 8a**). The spatial distribution of these genes across the tissue section recapitulated the expected zonation patterns (**Fig. 8b**). To validate the ability of Visium HD to capture zonation, we examined both a well-established periportal zonation marker (*HAL*) and a pericentral zonation marker (*CYP1A2*). Importantly, protein-level validation using immunohistochemistry (IHC) data from the Human Protein Atlas confirmed the zonated expression of these markers (**Fig. 8c**), supporting the ability of Visium HD to capture physiologically relevant spatial organization in the liver. Beyond sample C107, the other two Visium HD samples (C95 and C113), although lower quality, still capture the zonation of these markers (**Fig. 8d**). For C95, previously published Xenium data are also available, and *CYP1A2* was included in the 477 gene panel[6]. This further validated the zonation signal captured by Visium HD (**Fig. 8e**).

Usage Notes

An interactive Shiny app for exploring regions of interest are available at: faizanhasan20.github.io/VisiumHD-Liver
For two samples additional spatial and dissociated single-cell data have been published[6].

Data Availability

All data supporting this study are publicly available. Spatial transcriptomics data are deposited in GEO under accession GSE311383. Associated H&E images are available at https://doi.org/10.5281/zenodo.19609466

Code Availability

Reads were aligned and expression was quantified using Space Ranger (versions in Table 1). All analyses were performed in R (version 4.4.0). Bin annotation was carried out using Seurat (v5.3.0), spacexr/RCTD (v2.2.1), and BANKSY (v1.2.0). Graph-based analyses were performed using igraph (v2.1.4). Unless otherwise specified, analyses were run using default parameters.
All code for analysis presented here is available at: github.com/faizanhasan20/VisiumHD-Liver

Author Contributions

F.H., R.D.E., G.D.B., and S.A.M. conceived the study. F.H and R.D.E. performed data analysis. J.A., D.N., and C.T. contributed to investigation and data curation. A.R., B.S., I.M., G.D.B., and S.A.M. provided resources and supervision. F.H and R.D.E. drafted the manuscript with input from all authors. All authors reviewed and approved the final manuscript.

Competing Interests

Gary D. Bader advises and owns stock in Adela Bio. He advises BioRender. The remaining authors have no conflicts to report.

Acknowledgements

The authors acknowledge the University Health Network Pathology Research Program,the Advanced Optical Microscopy Facility and Princess Margaret Genomics Centre for their support and services. The concept figures were created with Biorender.com.

Funding

Research funded by a postdoctoral fellowship from Canadian Network on Hepatitis C (CanHepC). CanHepC is funded by a joint initiative of the Canadian Institutes of Health Research (CIHR) (NHC-142832) and the Public Health Agency of Canada (PHAC). As well as by a CIHR fellowship (FRN-201015) and an Ajmera Transplant Research Fellowship. Research also funded by grant numbers CZF2019-002429 and CZF2021-237921 and CZF2022-316558 (PPC) from the Chan Zuckerberg Initiative DAF, an advised fund of Silicon Valley and from CIHR grant HIT168002 (SAM, GDM, IDM, AR). Funds also provided by the University of Toronto's Medicine by Design, the Canada First Research Excellence Fund, Toronto General and Western Hospital Foundation and the UHN Foundation.

Bibliography

1. Devarbhavi, H. et al. Global burden of liver disease: 2023 update. J. Hepatol. 79, 516–537 (2023).
2. Andrews, T. S. et al. Single-Cell, Single-Nucleus, and Spatial RNA Sequencing of the Human Liver Identifies Cholangiocyte and Mesenchymal Heterogeneity. Hepatol. Commun. 6, 821–840 (2022).
3. van den Brink, S. C. et al. Single-cell sequencing reveals dissociation-induced gene expression in tissue subpopulations. Nat. Methods 14, 935–936 (2017).
4. Andrews, T. S. et al. Single-cell, single-nucleus, and spatial transcriptomics characterization of the immunological landscape in the healthy and PSC human liver. J. Hepatol. 80, 730–743 (2024).
5. Yu, S. et al. Spatial transcriptome profiling of normal human liver. Sci. Data 9, 633 (2022).
6. Edgar, R. D. et al. Single-cell atlas of human pediatric liver reveals age-related hepatic gene signatures. Hepatol. Commun. 9, (2025).
7. Edgar, R. (2025). H&E Images for Human Liver Visium HD. Zenodo. https://doi.org/10.5281/zenodo.19609466
8. van Der Hoeven, J. A. et al. Effects of brain death and hemodynamic status on function and immunologic activation of the potential donor liver in the rat. Ann. Surg. 232, 804–813 (2000).
9. Cable, D. M. et al. Robust decomposition of cell type mixtures in spatial transcriptomics. Nat. Biotechnol. 40, 517–526 (2022).
10. Singhal, V. et al. BANKSY unifies cell typing and tissue domain segmentation for scalable spatial omics data analysis. Nat. Genet. 56, 431–441 (2024).
11. Rappaport, A. M., Borowy, Z. J., Lougheed, W. M. & Lotto, W. N. Subdivision of hexagonal liver lobules into a structural and functional unit; role in hepatic physiology and pathology. Anat. Rec. 119, 11–33 (1954).
12. Yakubovsky, O. et al. A spatial atlas of the healthy human liver from live donors.

Nature (2026) doi:10.1038/s41586-026-10377-y.
13. Hao, Y. et al. Integrated analysis of multimodal single-cell data. Cell 184, 3573-3587. (2021).
14. Stuart, T. et al. Comprehensive Integration of Single-Cell Data. Cell 177, 1888-1902.e21 (2019).
15. Satija, R., Farrell, J. A., Gennert, D., Schier, A. F. & Regev, A. Spatial reconstruction of single-cell gene expression data. Nat. Biotechnol. 33, 495–502 (2015).
16. Antonov, M. et al. igraph enables fast and robust network analysis across programming languages. arXiv (2023) doi:10.48550/arxiv.2311.10260.
17. Hasan, F., Edgar, R.D., Bader, G.D., MacParland, S.A. GEO. https://identifiers.org/geo/GSE311383 (2026).

Figure Legends

Figure 1. Sample processing of human liver for Visium HD resulted in three samples of varying quality. (**a**) Sample processing workflow. (**b**) Quality metrics of three samples at three bin sizes. Values are labeled above bars that are too short to be read directly from the y-axis. (**c**) H&E staining of samples processed with Visium HD. (**d**) Location of 8 µm bins coloured by number of UMIs.

Figure 2. Annotation process for 8 µm bins of sample C107. (**a**) Workflow for cell annotation based on RCTD and BANKSY clustering when bins were rejected by RCTD. (**b**) Spot class output of RCTD. (**c**) Location of 8 µm bins coloured by RCTD spot class.

Figure 3. Expected cell types of the human liver can be captured, in their expected proportions and locations, using Visium HD. (**a**) Cell type annotation of the 8 µm bins. (**b**) Zoom-in of a representative central vein (CV) to portal vein (PV) axis. (**c**) Associated H&E staining of the same area. (**d**) Counts of 8 µm bins across the annotated cell types. (**e**) Correlation of cell type proportions between samples C107 and C95 (top) or C113 (bottom). Cell types are stratified based on whether they comprise more than 3% of total bins (right panels) to allow appropriate scaling. Pearson correlation coefficients and associated p-values are shown for each panel.

Figure 4. Expression of markers validates the cell type labels from the cell annotation pipeline. Gene expression of key markers used for cell type annotation. The colour of the points represents the gene expression level and size represents percent of cells of a type expressing the gene at all.

Figure 5. Lumen size can be quantified and associated with cell type composition. (**a**) Distribution of lumen sizes among 110 lumens identified in the tissue. (**b**) H&E staining of a representative region containing several lumens. (**c**) Association of bins by proximity to lumen of two sizes at the 8 µm bin resolution. (**d**) Percent of fibroblasts and hepatic stellate cells in regions adjacent (≤ 16 µm) or proximal (≤ 80 µm) to lumen across the entire tissue. *$p < 0.05$; two-way ANOVA.

Figure 6. Though sparse in counts the 2 µm bin resolution can capture endothelial lining at central veins not captured at the 8 µm bin resolution. (**a**) H&E staining of a representative central vein (CV). (**b**) Cell type annotation at the 2 µm bin resolution. (**c**) Further zoom-in on the representative CV with only those 2 µm bins annotated as endothelial highlighted. Points are coloured by endothelial cell type to highlight the distribution of vein endothelial cells (*TAGLN* and *SPARCL1* high) versus endothelial cells of pericentral hepatic sinusoid (*CLEC4G* and *LYVE1* high). (**d**) Cell type annotation at the 8 µm bin resolution. (**e**) Further zoom-in on the representative CV with only those 8 µm bins annotated as endothelial highlighted.

Figure 7. Bile ducts of different sizes can be identified. (**a**) Cell type annotation at the 8 µm bin resolution at representative periportal region. Transcriptionally identified bile ducts are highlighted with a black outlines. (**b**) H&E staining of a representative region with transcriptionally identified bile ducts are highlighted and coloured by size type. (**c**) Counts of cholangiocyte bins which were assigned to either small or large bile ducts.

Figure 8. Markers of zonation can be identified in the Visium HD expression data and

validated at the protein level. (**a**) Differential expression fold change of representative two zonated genes (*HAL* and *CYP1A2*). Fold change values compare all 8 µm Visium HD bins in a given zonation bin to all others for sample C107. (**b**) Expression of the two zonated genes across the entire C107 sample. (**c**) Representative IHC plots verifying zonation of these genes at the protein level. Annotations highlight portal veins (PV). (**d**) Expression of *HAL* and *CYP1A2* across the other two Visium HD samples (C95 and C113). (**e**) Expression of *CYP1A2* in the Xenium data available for C95.

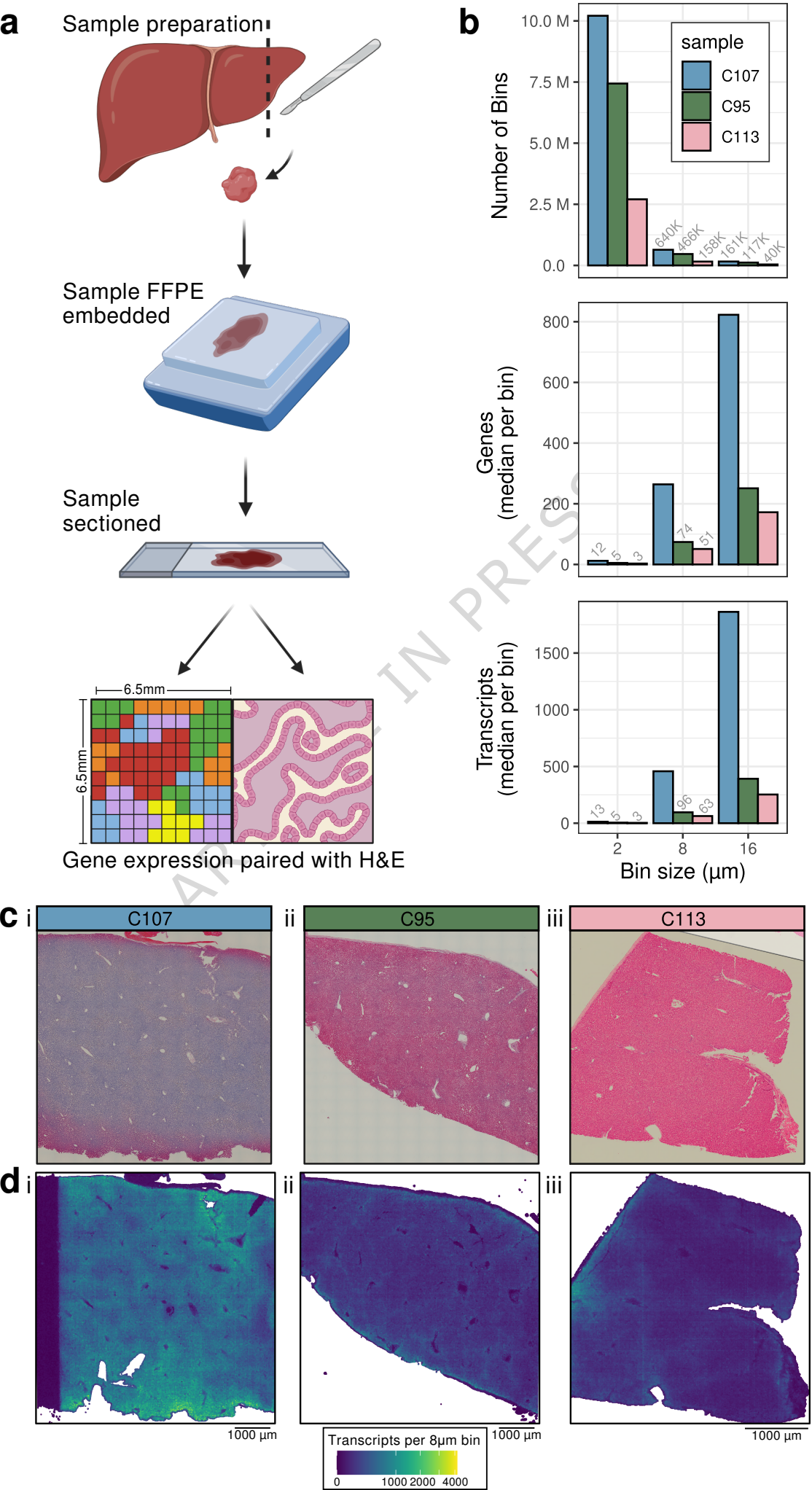

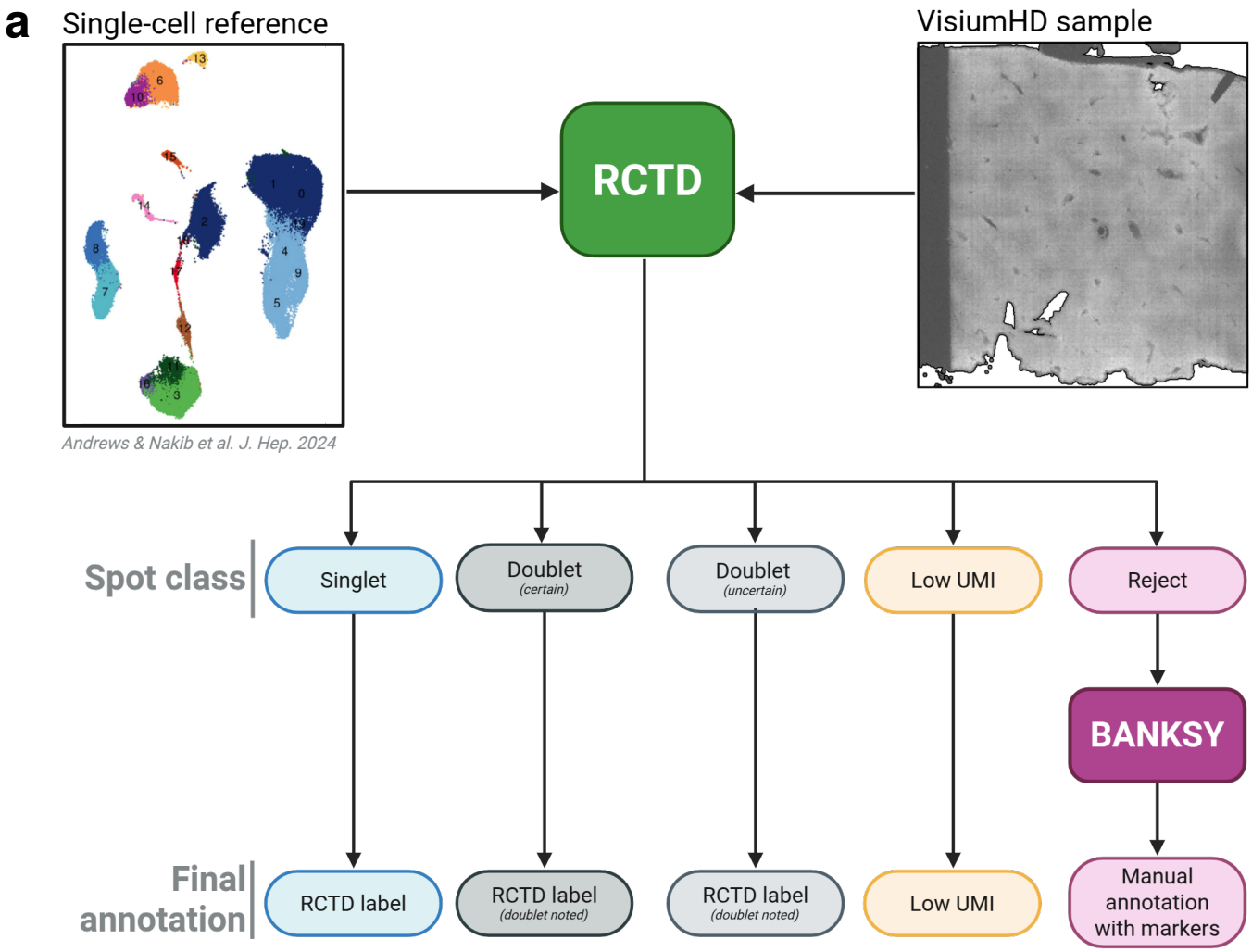
a
Single-cell reference
VisiumHD sample
RCTD
Andrews & Nakib et al. J. Hep. 2024
Spot class
Singlet
Doublet (certain)
Doublet (uncertain)
Low UMI
Reject
BANKSY
Final annotation
RCTD label
RCTD label (doublet noted)
RCTD label (doublet noted)
Low UMI
Manual annotation with markers

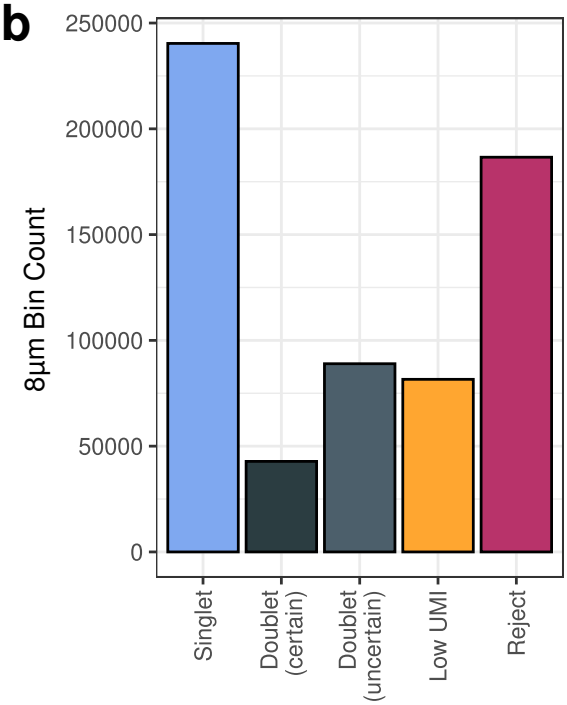
b
8µm Bin Count
250000
200000
150000
100000
50000
0
Singlet
Doublet (certain)
Doublet (uncertain)
Low UMI
Reject

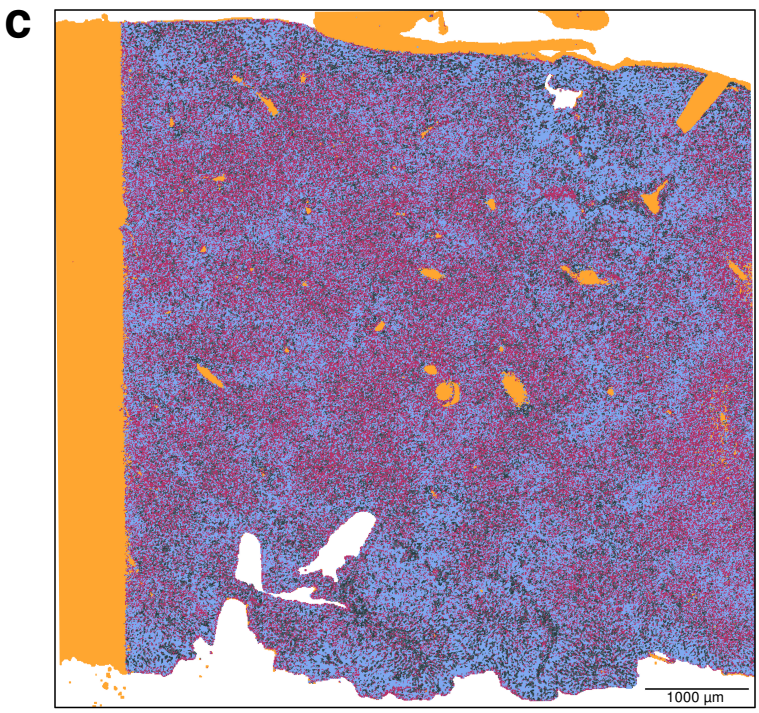
c
1000 µm

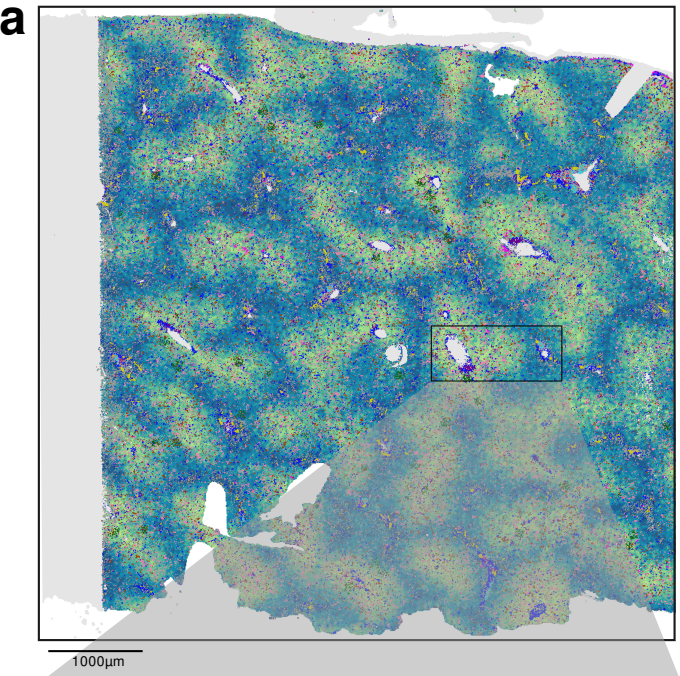

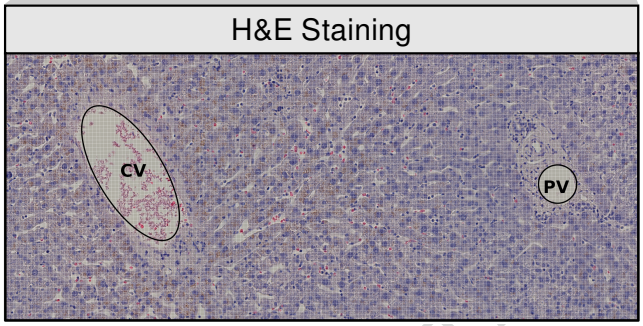

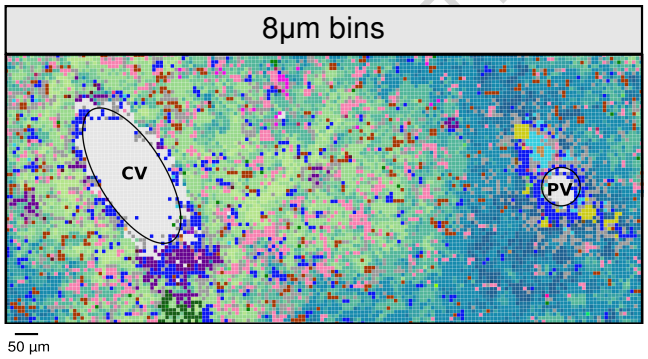

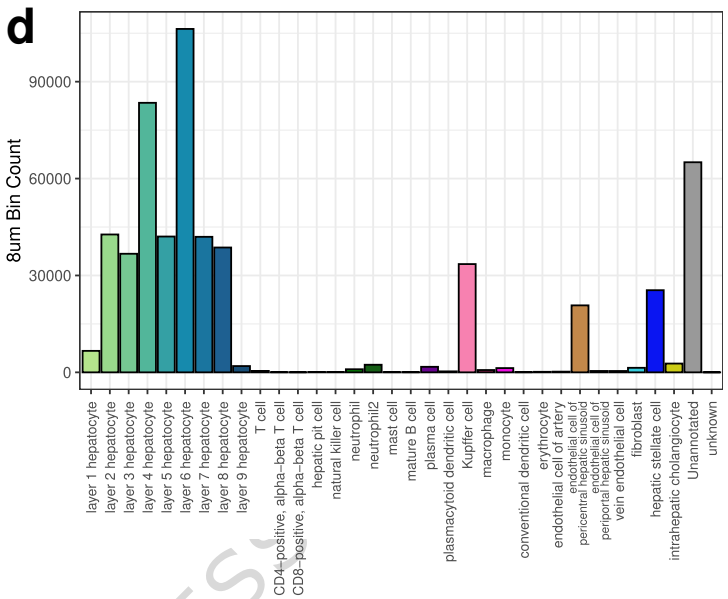

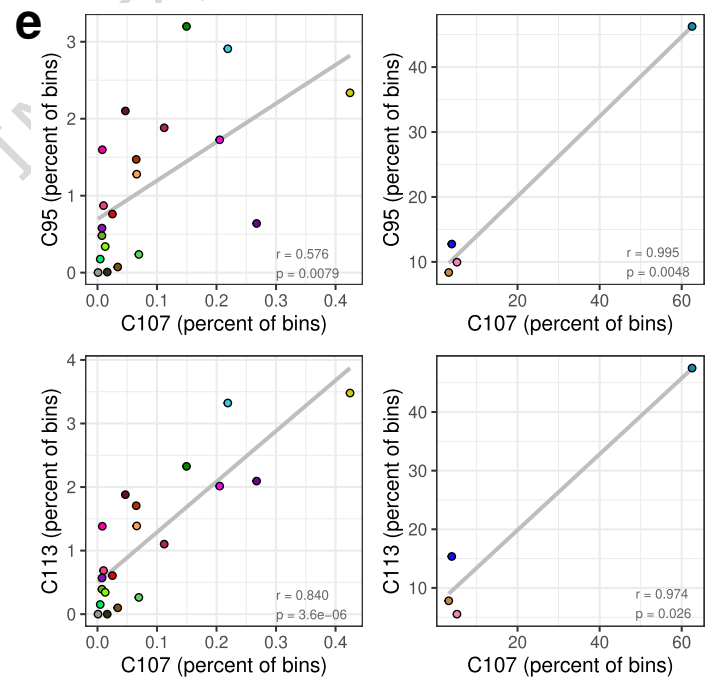

Cell Type

- macrophage
- conventional dendritic cell
- mast cell
- Kupffer cell
- monocyte
- intrahepatic cholangiocyte
- hepatic stellate cell
- fibroblast
- T cell
- CD4+ α-β T cell
- CD8+ α-β T cell
- natural killer cell
- neutrophil
- neutrophil2
- hepatic pit cell
- mature B cell
- plasma cell
- plasmacytoid dendritic cell
- erythrocyte
- vein endothelial cell
- endothelial cell of artery
- endothelial cell of pericentral hepatic sinusoid
- endothelial cell of periportal hepatic sinusoid
- Low UMI
- Unannotated

Hepatocyte types

- layer 1
- layer 2
- layer 3
- layer 4
- layer 5
- layer 6
- layer 7
- layer 8
- layer 9

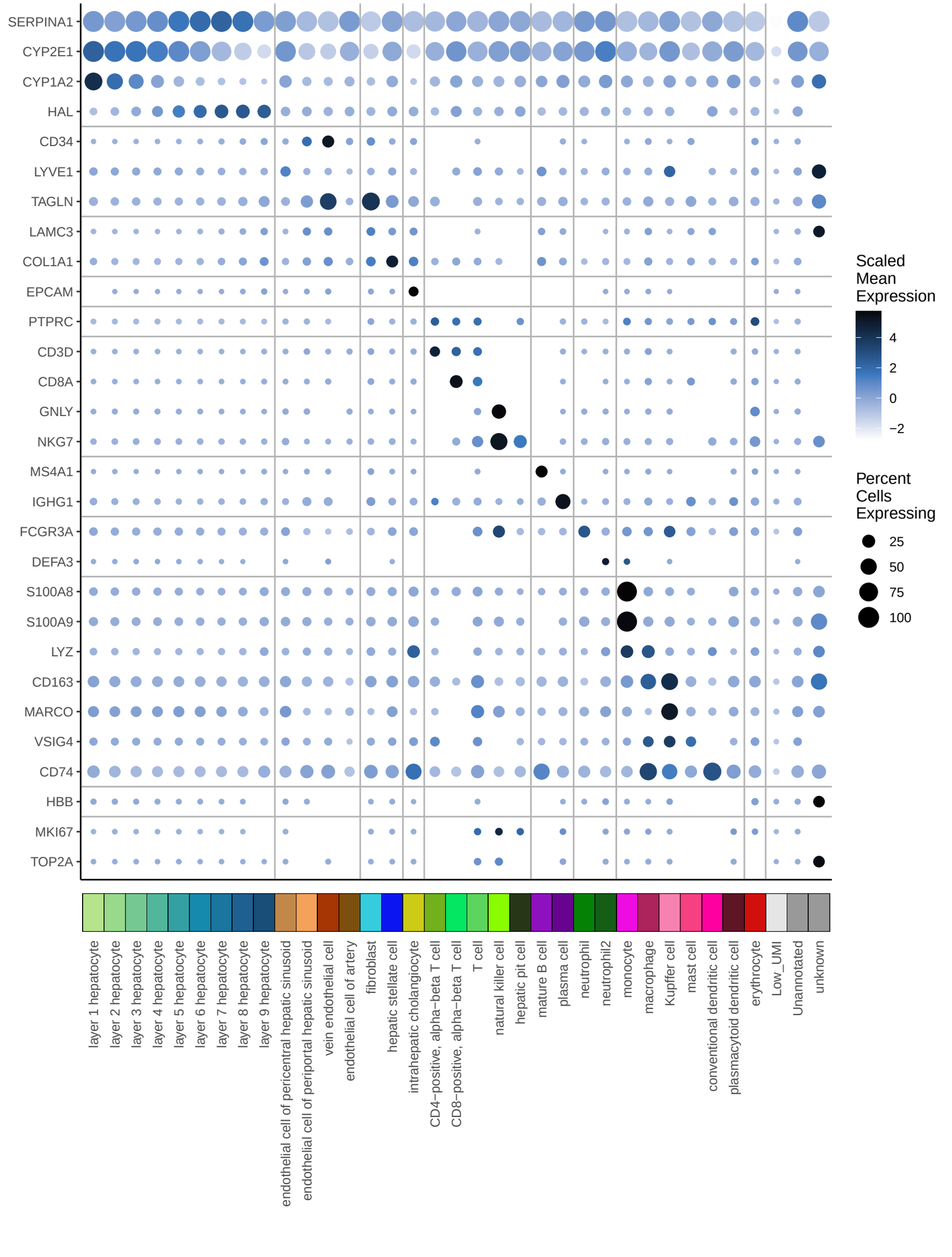
SERPINA1
CYP2E1
CYP1A2
HAL
CD34
LYVE1
TAGLN
LAMC3
COL1A1
EPCAM
PTPRC
CD3D
CD8A
GNLY
NKG7
MS4A1
IGHG1
FCGR3A
DEFA3
S100A8
S100A9
LYZ
CD163
MARCO
VSIG4
CD74
HBB
MKI67
TOP2A
Scaled Mean Expression
4
2
0
−2
Percent Cells Expressing
25
50
75
100
layer 1 hepatocyte
layer 2 hepatocyte
layer 3 hepatocyte
layer 4 hepatocyte
layer 5 hepatocyte
layer 6 hepatocyte
layer 7 hepatocyte
layer 8 hepatocyte
layer 9 hepatocyte
endothelial cell of pericentral hepatic sinusoid
endothelial cell of periportal hepatic sinusoid
vein endothelial cell
endothelial cell of artery
fibroblast
hepatic stellate cell
intrahepatic cholangiocyte
CD4−positive, alpha−beta T cell
CD8−positive, alpha−beta T cell
T cell
natural killer cell
hepatic pit cell
mature B cell
plasma cell
neutrophil
neutrophil2
monocyte
macrophage
Kupffer cell
mast cell
conventional dendritic cell
plasmacytoid dendritic cell
erythrocyte
Low_UMI
Unannotated
unknown

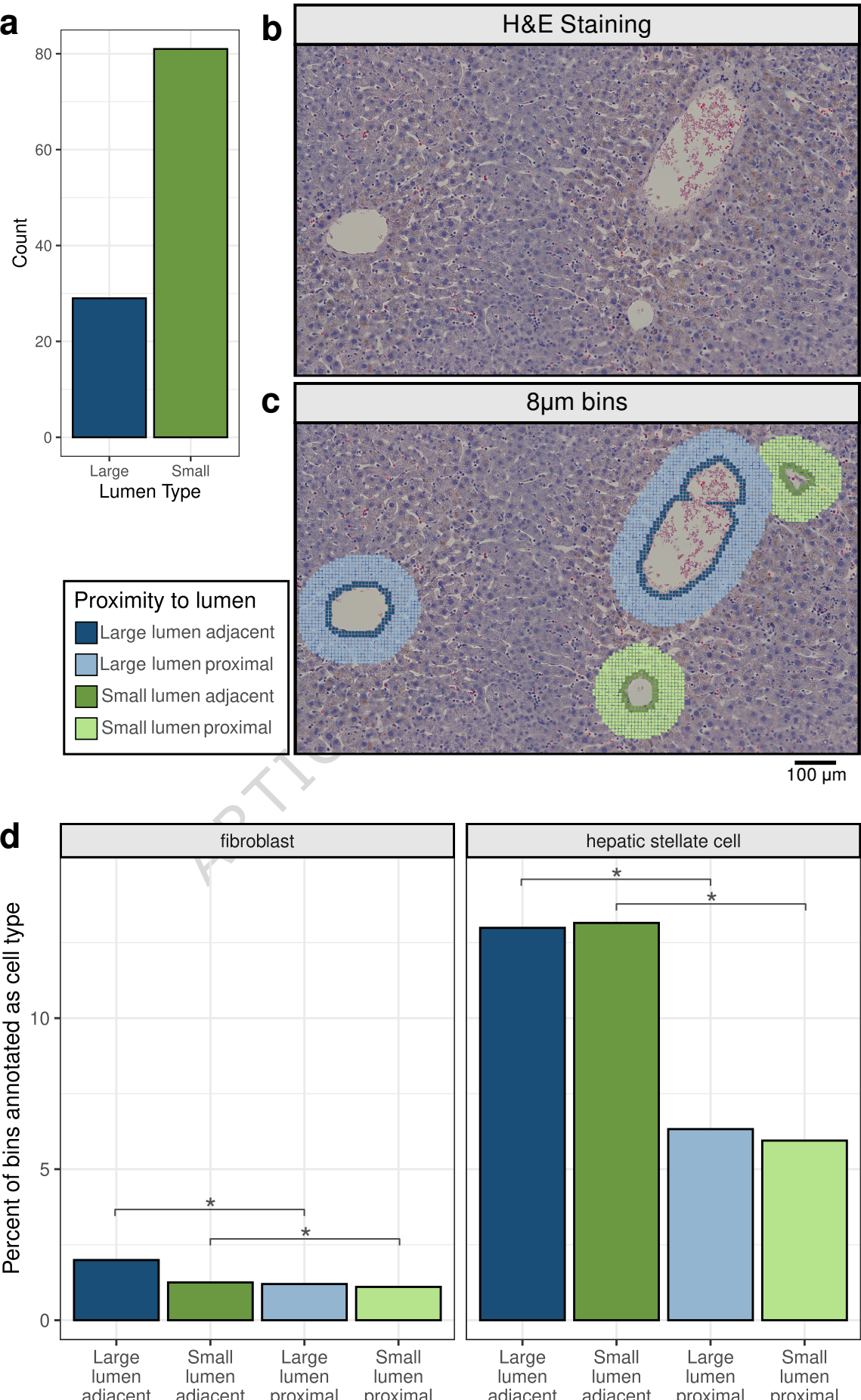
a
Count
80
60
40
20
0
Large
Small
Lumen Type
b
H&E Staining
c
8μm bins
Proximity to lumen
Large lumen adjacent
Large lumen proximal
Small lumen adjacent
Small lumen proximal
100 μm
d
Percent of bins annotated as cell type
fibroblast
hepatic stellate cell
10
5
0
*
*
*
*
Large lumen adjacent
Small lumen adjacent
Large lumen proximal
Small lumen proximal

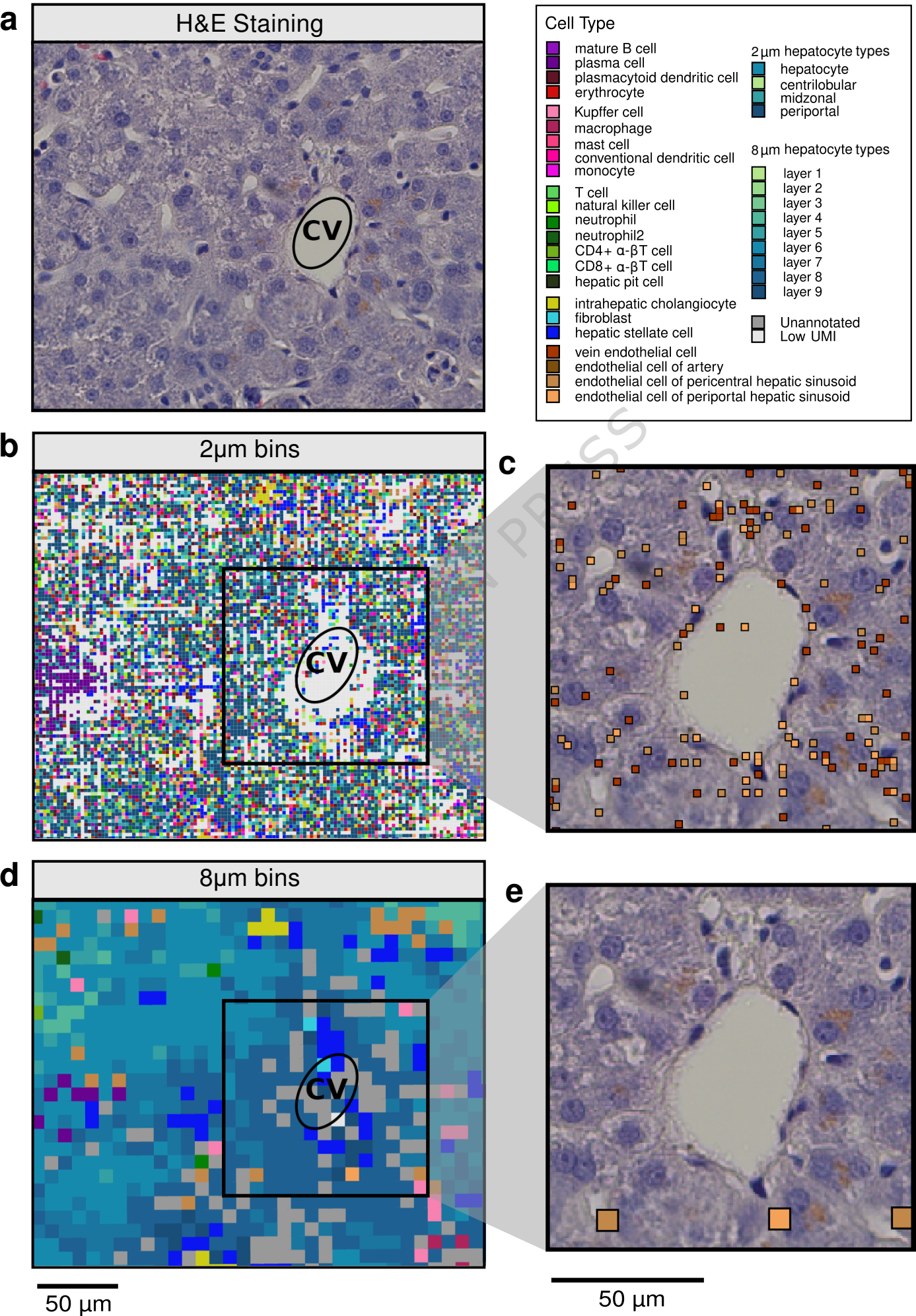

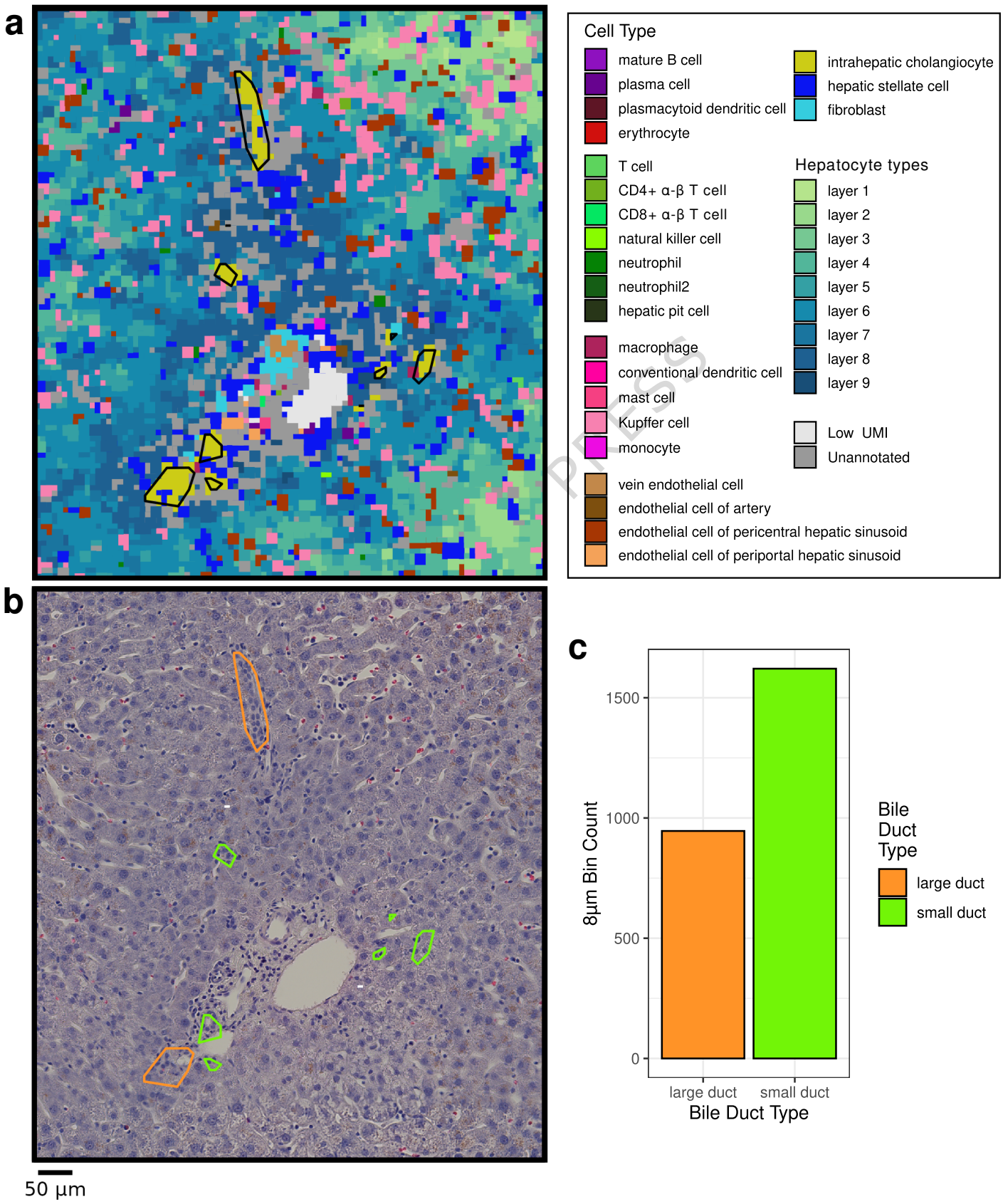
a
Cell Type
mature B cell
plasma cell
plasmacytoid dendritic cell
erythrocyte
T cell
CD4+ α-β T cell
CD8+ α-β T cell
natural killer cell
neutrophil
neutrophil2
hepatic pit cell
macrophage
conventional dendritic cell
mast cell
Kupffer cell
monocyte
vein endothelial cell
endothelial cell of artery
endothelial cell of pericentral hepatic sinusoid
endothelial cell of periportal hepatic sinusoid
intrahepatic cholangiocyte
hepatic stellate cell
fibroblast
Hepatocyte types
layer 1
layer 2
layer 3
layer 4
layer 5
layer 6
layer 7
layer 8
layer 9
Low UMI
Unannotated
b
50 µm
c
8µm Bin Count
1500
1000
500
0
large duct
small duct
Bile Duct Type
Bile Duct Type
large duct
small duct

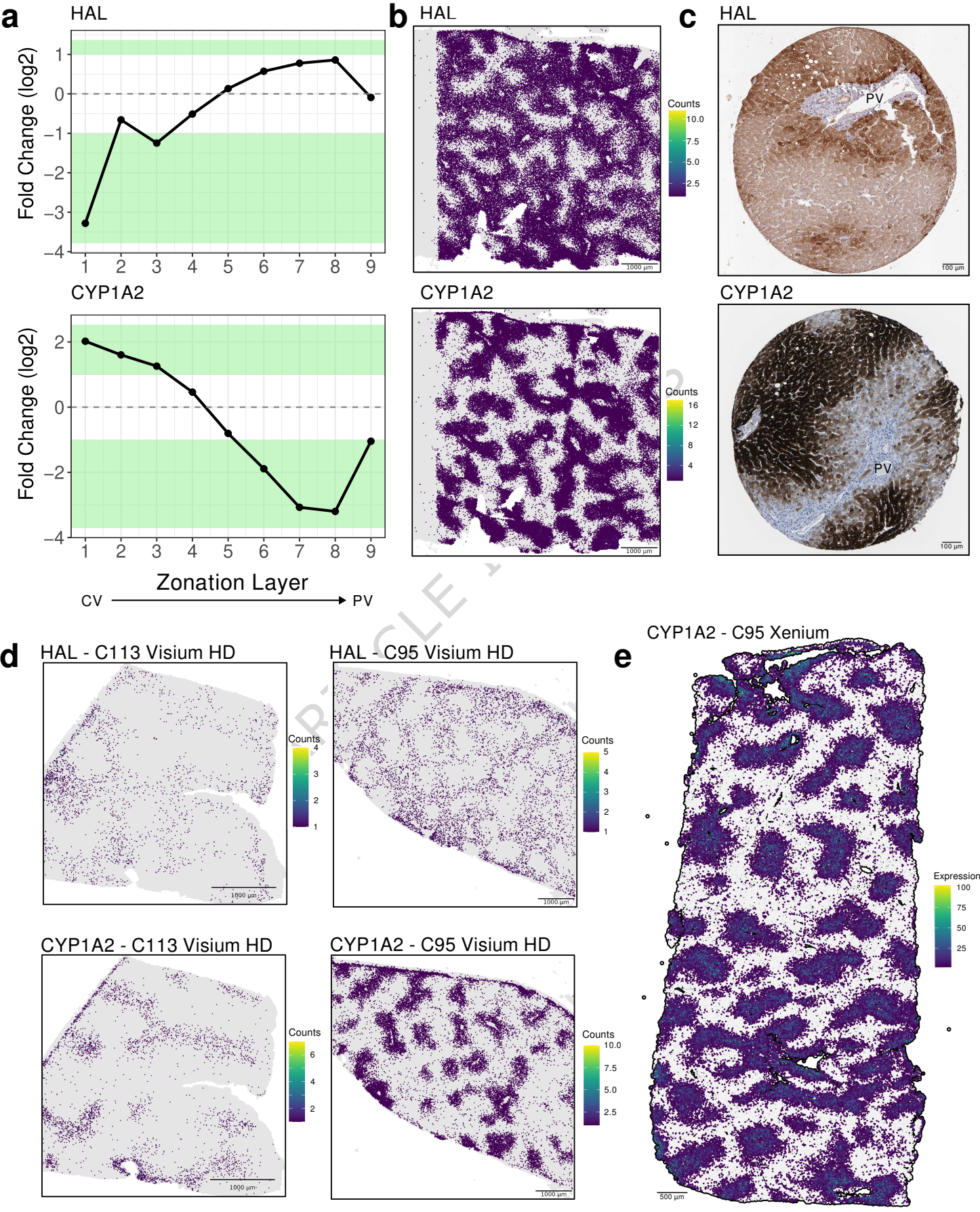
a
HAL
Fold Change (log2)
1
0
−1
−2
−3
−4
1 2 3 4 5 6 7 8 9
CYP1A2
Fold Change (log2)
2
0
−2
−4
1 2 3 4 5 6 7 8 9
Zonation Layer
CV
PV
b
HAL
Counts
10.0
7.5
5.0
2.5
1000 µm
CYP1A2
Counts
16
12
8
4
1000 µm
c
HAL
PV
100 µm
CYP1A2
PV
100 µm
d
HAL - C113 Visium HD
Counts
4
3
2
1
1000 µm
HAL - C95 Visium HD
Counts
5
4
3
2
1
1000 µm
CYP1A2 - C113 Visium HD
Counts
6
4
2
1000 µm
CYP1A2 - C95 Visium HD
Counts
10.0
7.5
5.0
2.5
1000 µm
e
CYP1A2 - C95 Xenium
Expression
100
75
50
25
500 µm